Chinese Chemical Letters 37 (2026) 112721

Contents lists available at ScienceDirect

Chinese Chemical Letters

journal homepage: www.elsevier.com/locate/cclet

MXene-based single-atom catalysis for enhanced Fenton-like reactions in water treatment

Zhitong Ma[a], Yuanfang Wang[b,*], Yajiao Wang[c], Xunli Wang[c], Qingbai Tian[d], Xing Xu[d,*], Hanghang Zhao[c,*]

[a] College of Geology and Environment, Xi'an University of Science and Technology, Xi'an 710054, China
[b] Department of Chemistry and Chemical & Environmental Engineering, Weifang University, Weifang 261061, China
[c] School of Chemical and Environment Science, Shaanxi University of Technology, Hanzhong 723001, China
[d] Shandong Key Laboratory of Water Pollution Control and Resource Reuse, School of Environmental Science and Engineering, Shandong University, Qingdao 266237, China

ARTICLE INFO

Article history:
Received 31 January 2026
Revised 25 March 2026
Accepted 2 April 2026
Available online 3 April 2026

Keywords:
MXenes
Single-atom catalysis
Fenton-like system
Catalytic devices
Pollutants

ABSTRACT

The application of MXene-based single-atom catalysts (SACs) in Fenton-like processes has emerged as a rapidly advancing research frontier in recent years. Early studies have demonstrated their superior activity in activating peroxymonosulfate or hydrogen peroxide for pollutant degradation compared to conventional nanoparticle catalysts, while recent efforts have shifted toward precise structural engineering and mechanistic understanding of reaction pathways. However, the transition from laboratory-scale synthesis to industrial implementation remains challenging, due to difficulties in developing green and scalable fabrication methods, long-term instability in complex water matrices, leaching of metal active centers, and the lack of cost-effective integration into continuous-flow systems such as fixed-bed reactors. To date, comprehensive reviews addressing their engineering applications remain limited. This review systematically summarizes advances in synthetic strategies and characterization techniques for achieving atomic dispersion, elucidates the structure–activity relationships and synergistic radical/non-radical mechanisms, and evaluates reactor design and scale-up potential. Particular emphasis is placed on operational adaptability and economic feasibility under real-world conditions. Future perspectives include the rational design of novel MXene supports, machine learning-assisted catalyst optimization, hybrid process integration, and the development of sustainability assessment frameworks, aiming to bridge the gap between fundamental discoveries and practical water purification technologies.

© 2026 Published by Elsevier B.V. on behalf of Chinese Chemical Society and Institute of Materia Medica, Chinese Academy of Medical Sciences.

1. Introduction

MXenes constitute an emerging class of two-dimensional materials composed of layered transition metal carbides, nitrides, or carbonitrides with the general formula $M_{n+1}X_nT_x$ (where M is a transition metal, X is carbon or nitrogen, and T_x represents surface functional groups) [1–4]. This structure endows MXenes with high specific surface area, excellent electrical conductivity, and tunable surface chemistry, making them highly suitable as supports for single-atom catalysts [3,5–9]. The synthesis of MXene-based single-atom catalysts typically begins with selective etching of $M_{n+1}AX_n$ phase (MAX) phase precursors to yield multilayer nanosheets, followed by post-treatment techniques such as impregnation or electrochemical deposition to anchor isolated metal atoms. These approaches leverage intrinsic defects and surface functionalities to prevent metal aggregation, thereby generating catalysts with high-density, well-defined active sites that enhance Fenton-like reaction efficiency [3,7,10–17].

The application of MXene-based single-atom catalysts in Fenton-like processes is a relatively recent yet rapidly advancing field (Fig. S1a in Supporting information). Initial explorations emerged around the late 2010s, coinciding with growing interest in both single-atom catalysis and MXene materials [3,5,6,10,14–19]. Early studies (*circa* 2018–2020) primarily served as proof-of-concept demonstrations, focusing on degrading model organic pollutants (*e.g.*, dyes, antibiotics) by activating peroxymonosulfate (PMS) or hydrogen peroxide (H_2O_2). These works established the superior activity of single-atom sites compared to traditional nanoparticle-based catalysts. In recent years (2021-present), research has evolved toward optimizing catalyst design and elu-

* Corresponding authors.
E-mail addresses: 20160024@wfu.edu.cn (Y. Wang), xuxing@sdu.edu.cn (X. Xu), zhaohh931106@163.com (H. Zhao).

https://doi.org/10.1016/j.cclet.2026.112721
1001-8417/© 2026 Published by Elsevier B.V. on behalf of Chinese Chemical Society and Institute of Materia Medica, Chinese Academy of Medical Sciences.

cidating reaction mechanisms [20–23]. Efforts have focused on engineering MXene's defect density, surface termination, and the coordination environment of metal centers to enhance stability, selectivity, and the activation efficiency for various oxidants (Fig. S1b in Supporting information). For example, Guo *et al*. developed the MXene with co-doping with CoN_1O_2 single-atom sites and Co nanoclusters for PMS activation with superior pollutant degradation [24]. Significant progress has been made in understanding the dominant role of radical/non-radical pathways, marking a shift from phenomenological observation to mechanistic understanding [3,25–29].

Translating MXene-based single-atom catalysts from laboratory research to industrial applications remains a major challenge in catalysis. In practical water treatment, an ideal catalyst must exhibit high activity, robust stability, ease of separation, and cost-effectiveness. Current efforts focus on integrating powdered catalysts into structured systems, such as aerogels, composite membranes, or fixed-bed reactors, to enable continuous-flow operation [26,28–34]. While pilot-scale studies have demonstrated efficacy in treating simulated wastewater, true industrial deployment faces three key barriers: Developing green and scalable synthesis methods, mitigating catalyst leaching and deactivation in real water matrices, and establishing comprehensive life-cycle assessment protocols [35–42].

To date, systematic reviews on the engineering application of these catalysts in Fenton-like systems remain incomplete. This review addresses this gap through a structured analysis of recent advances. It critically examines synthesis strategies and characterization techniques for achieving atomic dispersion, elucidates catalytic mechanisms and structure–activity relationships, and evaluates reactor integration and scale-up pathways. Particular attention is given to persistent challenges—including insufficient long-term stability, poor adaptability under real operating conditions, and economic constraints. Future directions are proposed, including the development of novel MXene supports, machine learning-assisted catalyst design, integration with hybrid technologies, and the establishment of scientifically sound sustainability metrics to advance the transition of fundamental discoveries into real-world applications.

2. Preparation and characteristics of MXenes-based SACs

2.1. HF etching approach

Among the diverse methodologies for synthesizing MXene-based single-atom catalysts, the HF etching approach remains a foundational technique [11,14,16,24,43]. This well-established process begins with selectively removing the A-layer (generally aluminum) from the MAX phase precursor, resulting in multilayered MXene nanosheets rich in surface functional groups such as -O, -OH, and -F. The presence of these terminations, along with inherent structural defects, offers favorable sites for anchoring metal precursors [11,44]. Subsequently, methods including wet impregnation, electrochemical deposition, or atomic layer deposition can be utilized to immobilize isolated metal atoms (such as Fe, Co, Cu, or Mn) onto the MXene substrate. This stage is essential for creating clearly defined, catalytically active single-atom centers, underscoring the HF etching route as a critical step in fabricating efficient MXene-supported single-atom catalysts [11,14,16,24,43].

The activation of PMS using various metal atoms anchored on Ti_3C_2-based MXene *via* etching has demonstrated effective removal of trace pollutants in water [16]. Xin *et al*. introduced an integrated etching–peeling–reduction approach to generate titanium vacancies, which served as anchoring sites for stabilizing cobalt single atoms on the MXene support (Co-SA/MXene) [16]. A marked increase in the interlayer spacing of $Ti_3C_2T_x$ MXene compared to the pristine MXene phase confirms the successful removal of the aluminum layer during etching. High-angle annular dark-field scanning transmission electron microscopy (HAADF-STEM) image combined with intensity profile analysis further corroborated the atomic dispersion of cobalt and reveals the coexistence of titanium vacancy defects induced by the etching process. Guo *et al*. synthesized the Co-SA/MXene catalyst *via* a multi-step etching strategy [24]. The Al layer of Ti_3AlC_2 MAX phase was selectively removed using HCl/LiF solution to yield MXene nanosheets, which were subsequently exfoliated by ultrasonication and subjected to H_2O_2-assisted etching to generate mesopores while preserving structural integrity. Zn^{2+} and Co^{2+} ions were then adsorbed onto the negatively charged MXene surfaces *via* electrostatic interactions. Following pyrolysis and acid leaching, well-dispersed CoN_1O_2 single-atom sites and Co nanoclusters were firmly anchored on the H_xMX support. Atomic force microscopy (AFM) revealed porous nanosheets with a thickness of ~1.6 nm, and the HAADF-STEM image clearly displayed atomic-scale cobalt species and nanoclusters embedded within the carbon matrix. Meng *et al*. utilized the etching strategy to achieve vacancy-mediated single-atom anchoring, resulting in the successful construction of a Co-N-$Ti_{3-x}C_2T_y$ catalyst featuring an asymmetric Co-N_1C_2 coordination environment (Figs. 1a and b) [43]. This unique structure simultaneously optimized electronic configuration, enhanced nano-confinement effects, and facilitated hierarchical mass transfer. The Co-N-$Ti_{3-x}C_2T_y$ catalyst was further fabricated into a catalytic membrane (Fig. 1c), with cross-sectional scanning electron microscopy (SEM) images exhibiting a uniformly stacked layered architecture with well-defined nanoscale interlayer gaps (Fig. 1d), offering abundant confined pathways for efficient fluid transport during the filtration-catalysis coupling process.

Basically, the etching strategy represents a viable route for constructing MXenes-based single-atom catalysts [3,45,46]. It introduces surface functional groups and defect sites during the selective removal of A-element layers, which can serve as anchoring points for metal atoms, allowing the integration of MXenes' favorable electrical conductivity and surface area with the high atomic efficiency of single-atom sites [3,45]. However, this approach faces notable challenges in safety and structural controllability: (i) The frequent use of corrosive reagents like HF raises safety and environmental concerns; restacking of MXene nanosheets during processing limits accessibility to active sites; and (ii) precise control over the single-atom loading process using impregnation or pyrolysis methods remains difficult, often resulting in nanocluster formation rather than uniformly dispersed single atoms, thereby compromising catalytic stability and performance reproducibility.

2.2. Alternative etching approach

Conventional HF etching, while fundamental to MXene synthesis, presents notable safety concerns owing to its use of concentrated hydrofluoric acid [47–49]. To overcome these limitations, researchers have engineered safer alternative methods that also afford superior structural precision [50,51]. These approaches prove essential for precisely tailoring the surface chemistry of MXene supports, critical to achieving effective single-atom anchoring. Among the promising techniques are electrochemical etching and alkali-assisted hydrothermal etching, both facilitating MXene fabrication under milder and better-controlled reaction environments [52]. A distinct advantage lies in their capability to fine-tune the variety and density of surface functional groups (–O, –OH) and defects. This control critically defines the coordination geometry of anchored metal single atoms, consequently regulating their electronic characteristics and catalytic behavior in Fenton-like reactions. For example, Guo *et al*. proposed an oxygen-rich surface termination strategy that promotes the formation of a

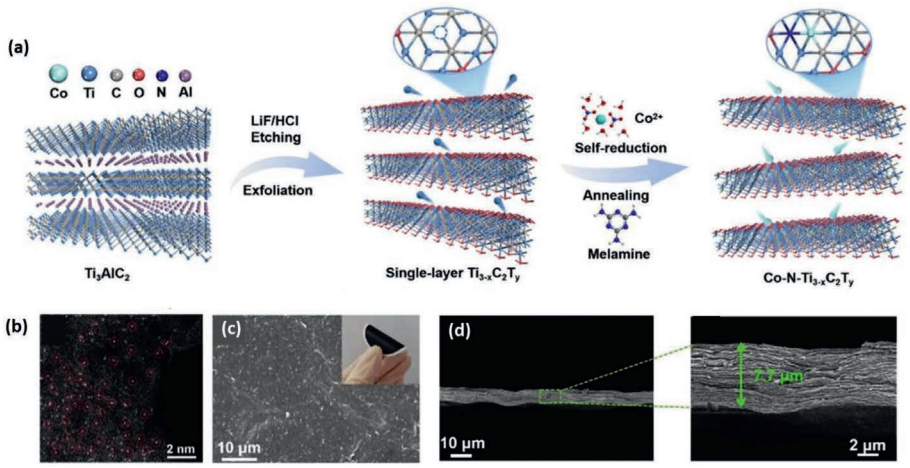


Fig. 1. (a) Fabrication scheme for Co-N-$Ti_{3-x}C_2T_y$ nanosheets. (b) HAADF-STEM analysis of Co-N-$Ti_{3-x}C_2T_y$ nanosheets. (c) SEM micrograph and optical image of the Co-N-$Ti_{3-x}C_2T_y$ membrane. (d) Cross-sectional SEM morphology of the Co-N-$Ti_{3-x}C_2T_y$ membrane. Reproduced with permission [43]. Copyright 2025, John Wiley and Sons.

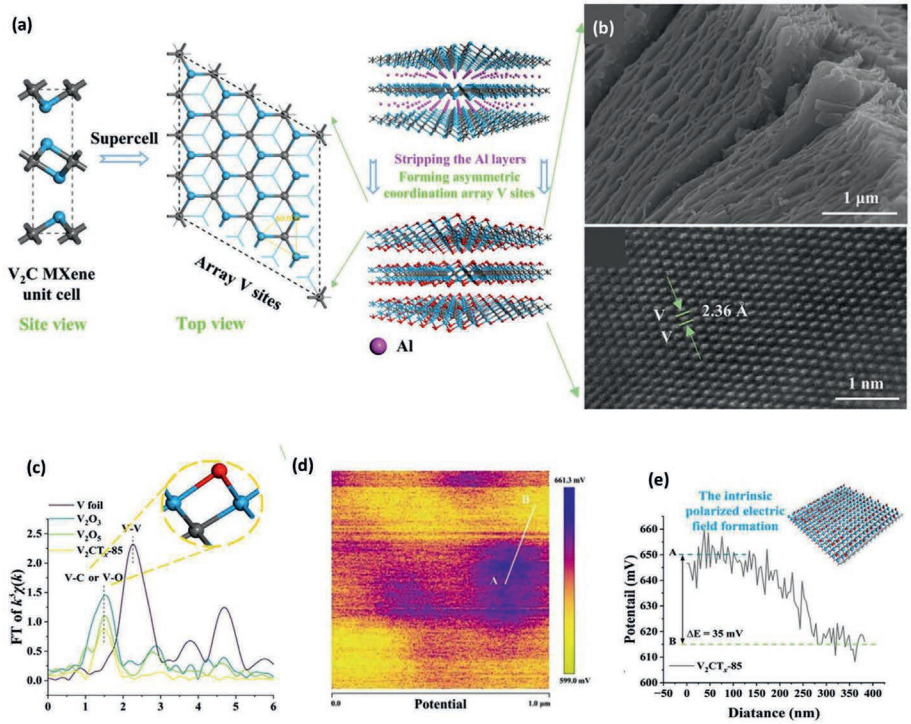


Fig. 2. (a) Schematic illustrations of the V sites and construction of TM sites with an asymmetric coordination array in MXene. (b) SEM and HAADF-STEM characterization of V_2CT_x-85. (c) Experimental k^3-weighted EXAFS spectra at the vanadium K-edge after Fourier transformation. (d) Nanoscale imaging of surface potential on V_2CT_x−85 by KPFM. (e) Variation of surface potential measured along the A–B path on V_2CT_x−85. Reproduced with permission [54]. Copyright 2025, Wiley-VCH.

stable metal–O–C structure, thereby significantly enhancing the activation efficiency of oxidants [53].

Etching methods that generate oxygen-rich terminations are crucial for establishing stable metal–O–C configurations, which are key to the efficient activation of oxidants [54,55]. Li *et al.* created asymmetric coordination array V sites on V_2C MXene using a wet chemical etch with NaF/HCl [54]. By optimizing the etching temperature to 85 °C, they introduced asymmetric V-O_{3-x}/V-$(OH)_{3-x}$ terminations (Fig. 2a). The material retained a periodic V-C-V lattice as well as densely ordered V arrays with a 2.36 Å interatomic spacing (Fig. 2b) [54]. Extended X-ray absorption fine structure (EXAFS) analysis at the V K-edge showed a dominant peak at 1.48 Å for V-O/V-C bonds, verifying the asymmetric coordination (Fig. 2c). Furthermore, Kelvin probe force microscopy (KPFM) measurements indicated a significantly stronger surface potential (Figs. 2d and e), confirming the creation of an intrinsic polarized electric field to enhance catalytic activity. In a separate approach, Li *et al.* developed a fluorine-free, alkaline hydrothermal method to produce high-purity $Ti_3C_2T_x$ MXene [56]. A concentrated NaOH solution at 270 °C etched the Al layer from Ti_3AlC_2, oxidizing and dissolving Al as $Al(OH)_4^-$ [57]. This process yielded MXene with dominant -OH/-O terminations and 92 wt% purity, establishing alkali etching as a sustainable alternative to fluorinated methods. Zhao *et al.* demonstrated a one-pot molten salt strategy using a $CuCl_2$/NaCl/KCl mixture to concurrently etch Ti_3AlC_2 and dope Cu^+ ions, directly fabricating Cu single-atoms on $Ti_3C_2T_x$ [58]. The Cu^+ ions were anchored by newly formed defects and -O terminations. HAADF-STEM confirmed atomic dispersion, and X-ray absorption

fine structure (XAFS) identified a Cu-O_4 coordination structure. This catalyst activated PMS with near-100 % singlet oxygen selectivity, showcasing the power of molten salt etching for the integrated engineering of catalyst support and active sites.

Collectively, these alternative etching methods provide a safer and more environmentally sustainable route by eliminating hazardous HF, while enabling unprecedented precision in tailoring MXene surface chemistry [59,60]. They facilitate the targeted introduction of abundant oxygen-containing functional groups and defects, thereby establishing an ideal platform for anchoring stable and highly active metal–oxygen–carbon single-atom sites. Nevertheless, significant challenges persist. Wet-chemical etching often lacks precise control over defect density and spatial distribution. Alkali-hydrothermal approaches typically require harsh reaction conditions, raising concerns about cost and scalability. Molten-salt etching may result in residual salts and non-uniform metal doping [60,61]. Moreover, the distinct surface microenvironments generated by different etching techniques complicate the universal prediction and fine-tuning of single-atom coordination configurations and catalytic performance. Future advances depend critically on developing synthesis strategies that are both controllable and scalable, coupled with a mechanistic understanding of how MXene etching conditions govern surface termination, atomic coordination, and ultimately catalytic performance, a causal chain essential for the rational design of high-performance catalysts [62,63].

2.3. Other synthesis methods of MXenes-based SACs

The synthesis of MXene-based single-atom catalysts has traditionally relied on etching methods. However, conventional etching techniques often face challenges in controlling site uniformity and avoiding structural damage or surface residues. This has driven interest in alternative non-etching approaches such as pyrolysis, electrodeposition, and atomic layer deposition [64]. These methods enabled precise metal atom anchoring while preserving the MXene framework. The resulting well-defined active sites could also enhance Fenton-like reactions by facilitating more efficient peroxide activation and electron transfer [7,65]. Pristine surfaces and engineered coordination environments further improve catalytic kinetics and stability, offering a robust platform for advanced water purification technologies.

In the non-etching preparation process, the direct synthesis method offers a way to fabricate MXenes that completely bypasses the etching step and enables precise control of the structure. Wang *et al.* reported a chlorine-terminated Ti_2CCl_2 MXene synthesized directly at high temperature from Ti, graphite, and $TiCl_4$, fully circumventing the traditional etching route (Fig. S2a in Supporting information) [66]. X-ray diffraction confirmed the formation of a pure-phase material with ideal chlorine termination, distinct from etched analogues that often exhibit chlorine deficiency. Scanning electron microscopy revealed large, well-aligned grains (Fig. S2b in Supporting information), while energy-dispersive spectroscopy mapping showed a uniform 1:1 distribution of Ti and Cl (Fig. S2c in Supporting information), confirming complete surface coverage. When synthesized optimally at 950 °C as a kinetic product, the material could be exfoliated into monolayers. This strategy provides a well-defined, fully terminated MXene platform without the need for hazardous etchants. Bai *et al.* synthesized CoSA-N_2O_1/MXene *via* pyrolysis of dicyandiamide, Co salt, and S-Ti_3C_2 nanosheets [67], as illustrated in Fig. S2d (Supporting information). Atomic dispersion of Co was well embedded in ultrathin sheet morphology (~2.68 nm) with the interatomic distance of ~0.322 nm based on the quantified through intensity profile analysis (Figs. S2e-g in Supporting information). The local coordination environment was identified by EXAFS fitting, which determined a Co-N_2O_1 configuration (Fig. S2h in Supporting information); this point has also been further confirmed by the corresponding density functional theory (DFT) optimized structural model (Fig. S2i in Supporting information). This asymmetric coordination could effectively modulate the electronic structure of the active sites, thereby improving their intrinsic activity for Fenton-like catalysis. Kuznetsov and colleagues introduced an atom substitution strategy to incorporate Fe single atoms directly into the Mo_2CT_x MXene framework, entirely bypassing conventional etching [68]. Structural analysis *via* HAADF-STEM verified the atomic dispersion of Fe, with no nanoparticle aggregation detected. X-ray absorption spectroscopy further identified Fe coordinated with N/O ligands, indicating a stable single-atom configuration. The resulting Fe–Mo_2CT_x catalyst exhibited high selectivity toward H_2O_2 generation *via* a two-electron oxygen reduction pathway.

Basically, the non-etching strategies mainly involve direct synthesis, pyrolysis-based anchoring, and atomic substitution, represent significant progress toward sustainable and controllable fabrication of MXene-based single-atom catalysts. These methods completely avoid the use of corrosive etchants, enabling the generation of active sites with precisely defined atomic configurations, pristine surfaces free from contamination, and adjustable coordination environments [68,69]. Such precise control over both electronic properties and spatial distribution of catalytic centers proves crucial for enhancing the activity, selectivity, and operational stability of Fenton-like reactions. However, scaling up these approaches presents considerable challenges [70]. Direct synthesis typically requires high-temperature and high-pressure conditions that are energy intensive. Meanwhile, pyrolysis-based methods often suffer from non-uniform precursor mixing and inadequate thermal control, which compromises reproducibility [71]. Future research should therefore prioritize improving scalability, cost-effectiveness, and process reliability of these synthesis routes to facilitate their transition from laboratory discovery to practical implementation.

3. Fenton-like performances and insights of MXenes-based SACs

During the synthesis of MXene-based single-atom catalysts, variations in process parameters, including preparation methods, etching conditions, temperature, and precursor composition, often lead to significant changes in single-atom configuration, such as coordination environment and loading density [2,7,11,14,24,67]. These structural differences affect the electron transfer efficiency between single-atom sites and the MXene support, as well as the strength of metal-support interactions. This subsequently influences the electronic structure of active sites and determines the selectivity between radical and non-radical reaction pathways, resulting in notable differences in pollutant degradation efficiency and reaction kinetics [2,7,18].

3.1. Radical with synergistic pathways

The integration of single-atom sites into the rigid, angstrom-scale channels of laminated MXene would create a powerful synergy that simultaneously revolutionized the catalytic activity and radical modulation [72]. Chen *et al.* engineered a Co single-atom catalyst anchored at Ti vacancies within a $Ti_3C_2T_x$ MXene laminate (Co-SA/MXene) [72]. Atomic-scale activation was achieved through an asymmetric Co-N_1O_2 coordination, which optimized electron donation to PMS. This was coupled with a physical nanoconfinement effect from the uniform ~0.35 nm interlayer spacing, which drastically enriched reactant concentrations and curtailed radical diffusion distances (Fig. 3a). This atomic-nano synergy yielded an extraordinary catalytic activity for ranitidine oxidation, far surpassing control systems (Fig. 3b). The synergy resulted in a record-high apparent rate constant of 3.4×10^4 min^{-1}, representing a 4–6

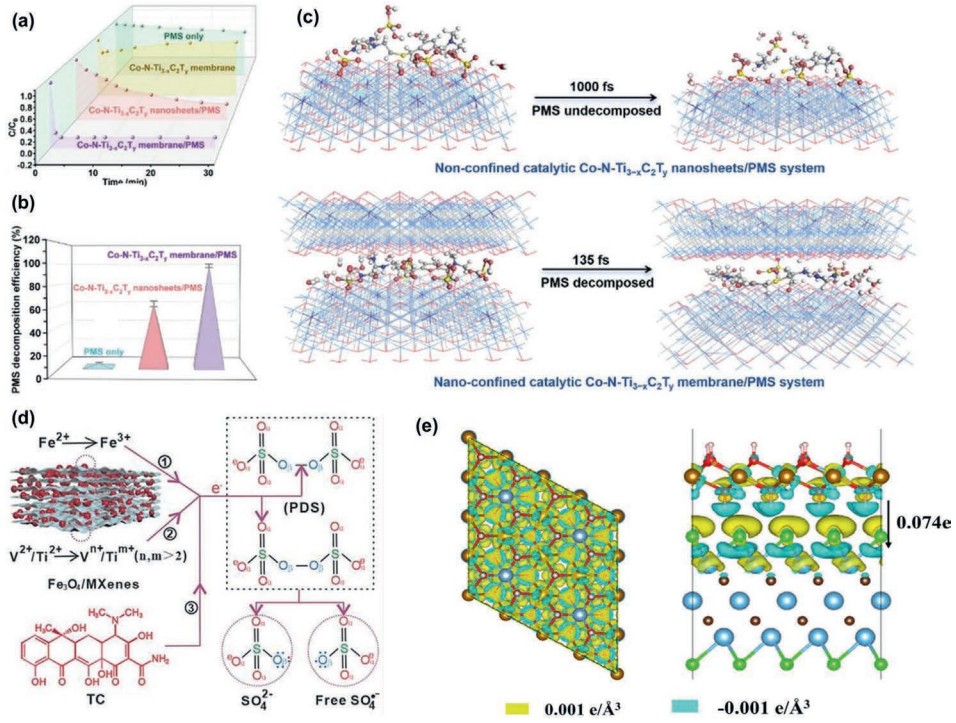


Fig. 3. (a) Catalytic activity for ranitidine oxidation in varied systems. (b) Oxidant consumption profiles in different catalytic systems. (c) AIMD simulations unravel nanoconfinement effects through comparative reactant trajectory analysis. Reproduced with permission [72]. Copyright 2025, Wiley-VCH. (d) Electron transfer pathways to PDS. Reproduced with permission [74]. Copyright 2025, Elsevier B.V. (e) Structural and electronic insights into the MXene/Fe–Al LDH interface. Reproduced with permission [75]. Copyright 2025, Elsevier B.V.

order-of-magnitude enhancement over conventional slurry reactors for radical generation. Ab initio molecular dynamics (AIMD) simulations visually unraveled this enhancement, showing the confined trajectory and rapid decomposition of PMS molecules within the nanochannel (Fig. 3c), compared to their bulk-phase diffusion. This principle could also be observed in other nanoconfined systems where tailored pore sizes (*e.g.*, sub-2 nm) are critical for maximizing radical exposure and reaction kinetics [72,73].

Constructing an electronic interface between MXenes and catalytic sites is an effective strategy to direct radical reaction pathways towards more efficient, surface-confined transformation processes. Wang *et al.* reported an iron-based V_2C MXene composite, in which V_2C MXene acted as an electronic medium, significantly promoting the interfacial electron transfer between the catalyst and peroxodisulfate (PDS) [74]. First-principles calculations indicated that the electron transfer from the composite to PDS amounts to 0.303 e^-, accompanied by a notable elongation of the O–O bond in PDS (Fig. 3d). This electronic interaction not only accelerated the activation of surface-adsorbed PDS but also promoted the *in-situ* generation of radicals such as $SO_4^{\bullet-}$ and $^{\bullet}OH$ on the catalyst surface. Thanks to the uniform anchoring of iron species on the V_2C surface and the layered MXene confinement structure, the generated radicals were effectively localized near the catalyst-solution interface, forming a high concentration of "surface-bound" active species. Quenching experiments and kinetic analysis confirmed that these interface-bound radicals contribute >45 % to the degradation of tetracycline. This interface engineering strategy effectively suppressed the diffusion and self-quenching of radicals in the bulk solution, significantly enhancing their spatial utilization efficiency and reaction selectivity [74].

Constructing hybrid active sites that combined the single atoms with tailored supports or co-catalysts introduced a profound electronic synergy for radical generation [3,7,14,75,76]. Yang *et al.* discovered a MXene/Fe-Al layered double hydroxide (LDH) mixed system, in which the electronic structure was of crucial importance at the heterojunction interface [75]. The top-view electron density difference map revealed clear charge redistribution upon hybridization, indicating strong interfacial electronic coupling (Fig. 3e). The corresponding side-view model illustrated the integrated atomic structure, where the MXene and Fe-Al LDH layers were closely associated with an interlayer distance of approximately 0.32 nm. This intimate contact facilitated continuous charge transfer across the interface. The synergy modulates the adsorption and activation of PMS, favoring the generation of multiple radical species ($SO_4^{\bullet-}$, $^{\bullet}OH$) and non-radical $^1O_2$ in a concerted manner. Consequently, the hybrid catalyst could achieve a 98.7 % degradation efficiency of bisphenol A (BPA) within 10 min, with a rate constant 5.1 times higher than that of the pristine LDH. This work underscores that beyond single-atom sites, crafting synergistic interfaces between different functional components on MXenes is a versatile strategy to create complex, high-performance radical-generation systems.

3.2. Other catalytic pathways in MXene-based SACs

Beyond radical–dominated pathways, MXene-supported single-atom catalysts can also mediate non-radical reaction mechanisms, offering enhanced selectivity and greater resilience to variable water matrix conditions [67]. These pathways, primarily involving singlet oxygen ($^1O_2$) generation and high-valent metal-oxo species ($M^{(n+1)}$=O) formation, were governed by precise atomic-level engineering of the metal center's coordination and electronic coupling with the MXene support [67,77].

The catalytic activity and pathway selectivity are fundamentally determined by the electronic structure of the single-atom sites, which can be directly engineered through the MXene support [16]. Xin *et al.* constructed a cobalt monometallic catalyst (Co-SA/MXene) on Ti_3C_2 MXene through titanium vacancy engineer-

ing, which was able to create a unique coordination environment [16]. Theoretical calculations revealed that the introduction of vacancies drastically modulated the local density of states of the Co site and altered the contribution of Ti 3d and C 2p orbitals to the frontier bands (Figs. S3a and b in Supporting information), a key electronic feature visualized in the projected density of states and orbital contribution analysis [16]. This engineered electronic structure was not merely a static property; it also enabled the catalyst to steer the activation of PMS toward a specific reaction channel. By optimizing the electron density at the active site, the adsorption and cleavage mode of the O–O bond in PMS could be precisely controlled, shifting the balance between different reactive oxygen species and ultimately determining whether $^1O_2$ or $M^{(n+1)}$=O became the dominant species for pollutant degradation.

The generation of high-valent metal-oxo species ($M^{(n+1)}$=O) provides a selective, robust, and mechanistically distinct alternative to conventional radical-based oxidation in water treatment [54]. This non-radical pathway could be successfully realized through the rational design of asymmetric coordination arrays on V_2CT_x MXene, where the precisely tailored V-O_x coordination geometry governs both the thermodynamic favorability and kinetic efficiency of $M^{(n+1)}$=O formation. This specific local geometry would reconstruct the electronic structure of the vanadium center, lowering the energy barrier for the heterolytic cleavage of the PMS O–O bond to trigger the formation of a transient $V^{(n+1)}$=O species as the primary species for degrading BPA (Fig. S3c in Supporting information) [54]. The degradation kinetics showed a strong, linear correlation with the tailored electronic potential of the active site, establishing this potential as a key descriptor for predicting activity (Fig. S3d in Supporting information). Importantly, the system exhibited excellent operational stability, maintaining high BPA removal efficiency over consecutive reaction cycles based on the oriented activation of PMS at the asymmetric site to generate the $V^{(n+1)}$=O species (Figs. S3e and f in Supporting information).

In fact, the exceptional performance of MXene-based SACs stemed from a synergistic orchestration of multiple pathways, elegantly leveraging the intrinsic properties of the MXene architecture [78,79]. Gao *et al.* discovered an independent catalytic membrane in which cobalt atom ions were embedded within the $Ti_3C_2T_x$ nanosheets [79]. These atomic ions possessed coordinatively unsaturated Co-N_1O_2 sites. This design achieved a powerful dual function: The atomic sites concurrently activated PMS to generate reactive species like $^1O_2$ and $M^{(n+1)}$=O, while the two-dimensional nanochannels formed by the stacked MXene layers would enforce the rapid mass transport and nanoconfinement effects. This synergistic combination of atomic-scale catalytic activation and nanofluidic mass transport enabled rapid water purification, achieving complete degradation of recalcitrant pollutants such as carbamazepine within 240 milliseconds (ms) while maintaining high membrane flux. These findings demonstrated how precisely engineered atomic-scale features, when integrated with macroscopic system design, can substantially advance the performance limits of catalytic membrane systems.

However, the rational design of such integrated systems for specific reaction pathways presented a complex multivariate challenge, as catalytic outcomes depend critically on the interplay of metal species, local coordination environment, and MXene substrate characteristics. Addressing this high-dimensional design problem requires approaches that transcend conventional empirical methods. Machine learning (ML) provides a powerful methodological framework for this purpose. When trained on comprehensive datasets incorporating synthesis conditions, atomic-level characterization data, and catalytic performance metrics, ML models can identify non-obvious structure-activity correlations, predict optimal material compositions, and guide the inverse design of next-generation MXene-based SACs tailored for efficient water purification applications, which would be analyzed in subsequent section.

4. ML-driven single-atom catalysis on MXene

The convergence of materials science and data science has positioned ML as a transformative tool in the rational design of MXene-based SACs [32,80–89]. By integrating diverse datasets (such as spanning synthesis conditions, structural features, and catalytic performances), ML models can decode complex structure–property relationships that are often obscured in conventional analyses. This capability enables reliable prediction of key metrics such as activity, selectivity, and stability.

It should be pointed out that no ML-driven studies have yet been reported specifically for MXene-based SACs in advanced oxidation processes (AOPs), successful applications in adjacent domains, such as electrocatalysis, CO_2 reduction, and hydrogen evolution reaction, demonstrate the transferability of these strategies [90,91]. Lin *et al.* integrated feature engineering with supervised machine learning to identify atomic-scale descriptors that quantitatively govern both single-atom anchoring energy and key reaction barriers [91], enabling rational, descriptor-driven design of MXene-based SACs for electrocatalytic nitrogen fixation (Fig. 4a). Their work exemplified how ML shifted development from empirical trial-and-error toward targeted design. In related efforts, the same groups employed generative adversarial networks (GANs) and graph neural networks (GNNs) to construct virtual libraries of MXene-supported architectures with tailored coordination environments [91]. These in silico libraries were then screened *via* high-throughput computation to pinpoint optimal metal centers and local geometries. Moreover, ML can optimize synthesis pathways by predicting the influence of factors such as etching conditions, thermal treatment temperature, and precursor ratios on the final structure, thereby improving the controllability and reproducibility of the fabrication process. A particularly promising direction was the integration of ML with automated experimental platforms to form a closed-loop workflow of "computational prediction → experimental validation → feedback optimization" (Fig. 4b), enabling rapid iteration and performance enhancement of catalysts. These underlying workflows, descriptor frameworks, and model architectures developed in those contexts could provide a solid foundation for future AOP-focused investigations.

Despite its considerable potential in catalyst design, the advancement of ML faces challenges related to data quality, model interpretability, and cross-scale correlation. Future research should dedicate efforts to constructing standardized, open-access MXene-SACs databases, developing interpretable ML models that balance predictive power with physical meaningfulness, and fostering deeper integration of multi-scale simulations with experimental data. By strengthening interdisciplinary collaboration among materials science, chemistry, environmental science, and artificial intelligence, ML will not only expedite the discovery of high-performance MXene-SACs but also hold promise for building intelligent catalytic systems. This integration aims to achieve precise control and autonomous optimization of water treatment processes, ultimately driving the field from fundamental research toward intelligent and sustainable practical applications.

5. Catalytic devices of MXenes-based SACs

Bridging the gap between fundamental catalytic mechanisms and real-world applications demands the engineering integration of catalysts into functional devices (Fig. 5), which is a central requirement for deploying Fenton-like catalysis in practice [31]. Accordingly, constructing macroscopic catalytic devices using MXene-supported single-atom catalysts is essential to enable

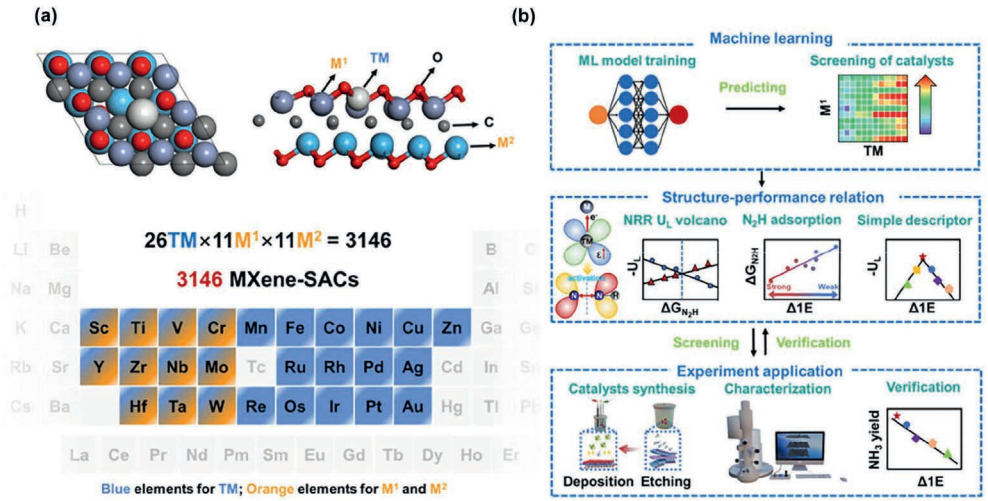


Fig. 4. (a) Structural blueprint of the MXene-SAC hybrid system. (b) Rational design workflow integrating computation and automation. Reproduced with permission [91]. Copyright 2025, American chemical society.

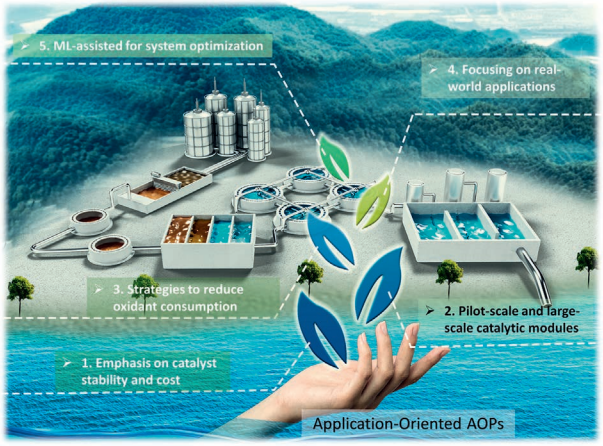


Fig. 5. Key directions in the application-oriented AOPs systems. Reproduced with permission [31]. Copyright 2025, American chemical society.

efficient, continuous-flow water treatment. By embedding atomically dispersed active sites within structured supports, such as three-dimensional porous monoliths or two-dimensional separation membranes, these devices synergistically couple molecular-scale activation with accelerated mass transport [13,92,93]. This architecture directly addresses key limitations of conventional powder catalysts, including poor recoverability, operational instability under flow conditions, and difficulty in process scale-up, thereby delivering water purification performance that is both reliable and amenable to industrial implementation [36,94–97].

A primary challenge in applying nanoscale catalysts is their difficult recovery from treated water. Yang *et al.* fixed single-atom copper (Cu-SA) onto two-dimensional MXene nanosheets [7], and then assembled them onto a polymer substrate (Figs. S4a-c in Supporting information). The resulting freestanding membrane exhibited a dense, layered internal structure, which was essential to its function for PMS activation. The atomic Cu–O_3 coordination sites enabled a distinct reaction pathway, activating PMS with nearly 100% selectivity toward $^1O_2$ generation. This non-radical mechanism offered superior resistance to common water matrix interferents. When evaluated in a continuous-flow system, the membrane device maintained stable performance in degrading BPA, achieving high removal efficiency and significant mineralization. This work demonstrated a successful fusion of SAC selectivity with membrane-based process engineering, enabling targeted and robust decontamination under dynamic flow conditions. Wu *et al.* developed a monolithic catalytic device by embedding Co-doped MXene (CoMX) into a macroporous chitosan aerogel matrix [11]. This design yielded a freestanding, mechanically robust block with a well-defined, interconnected pore network, as seen in its cross-sectional morphology (Figs. S4d and e in Supporting information), facilitating rapid fluid flow and pollutant access. The aerogel could effectively immobilize atomically dispersed cobalt catalysts, preventing their loss during operation. In addition, its monolithic architecture enabled easy retrieval and reuse, with high degradation efficiency retained over multiple cycles. This approach demonstrated a practical pathway for translating SACs into robust, recyclable treatment units through three-dimensional macrostructuring.

A further advancement was realized through vacancy-engineered monolithic SAC membranes. In this design, cobalt single atoms were first anchored at titanium vacancy sites on MXene nanosheets, which were then assembled into a rigid laminated membrane [72]. The resulting architecture featured sub-nanometer confined channels that generated a pronounced nanoconfinement effect. In addition, the membrane exhibited an exceptional combination of performance metrics in a continuous-flow configuration (Fig. S4f in Supporting information): It achieved an unprecedented apparent rate constant for pollutant oxidation—exceeding 50,000 min^{-1}—while simultaneously delivering ultrahigh water flux (Figs. S4g and h in Supporting information). This simultaneous improvement in both catalytic activity and membrane permeability successfully overcame the long-standing trade-off between these two critical performance metrics. As illustrated in Fig. S4i (Supporting information), the integrated process synergistically combined PMS activation, nanoconfined oxidative degradation, and selective membrane separation. Furthermore, atomic-scale anchoring of catalytically active sites conferred exceptional operational stability, with negligible metal leaching (<0.1 ppm) detected over 120 h of continuous operation. Collectively, these designs represented a paradigm shift in membrane-based water treatment, transforming the membrane from a passive separation barrier into an atomically engineered, high-efficiency catalytic reactor [98–100].

However, the practical implementation of MXene-based SACs continues to face several critical challenges, despite their promising catalytic performance. A primary obstacle lies in the limited preci-

sion of scalable synthesis techniques in controlling single-atom anchoring sites on MXene substrates, often resulting in metal aggregation or inconsistent active site density. Furthermore, the structural vulnerability of MXene under oxidative or aqueous conditions promotes carrier degradation and active species leaching, substantially compromising long-term operational stability. The interplay among MXene surface chemistry, intrinsic defects, and metal–support interactions also remain inadequately understood, impeding rationally guided catalyst design. In realistic water treatment contexts, the long-term efficacy and stability of these catalysts in the presence of natural organic matter, coexisting ions, and suspended particles require further systematic validation. Moreover, although most current studies are conducted under batch or simplified flow configurations, scaling up to stable, continuous-flow, and low-energy modular systems requires coordinated progress in catalyst design, reactor architecture, and operational optimization.

6. Conclusions and perspectives

MXene-supported single-atom catalysts demonstrate remarkable catalytic activity, tunable reaction pathways, and structural stability in Fenton-like reactions, offering a promising platform for advancing water treatment technologies. This review comprehensively summarizes recent progress in the synthesis strategies, structural characteristics, reaction mechanisms, and device integration of such catalysts, with particular emphasis on the synergistic interactions between atomically dispersed active sites and MXene supports. These interactions contribute to improved oxidant activation efficiency and accelerated pollutant degradation kinetics. Research indicates that strategies including defect engineering, surface terminal group modulation, and etching-free synthesis enable precise anchoring of single-atom sites and fine-tuning of their electronic structures. Such control facilitates selective regulation of radical and non-radical pathways, steering catalytic reactions toward higher efficiency, enhanced selectivity, and reduced energy consumption.

Nevertheless, practical implementation of these catalysts faces several challenges. First, green and scalable synthesis methods remain underdeveloped. Achieving high metal loading and uniform single-atom distribution without aggressive etchants presents a significant hurdle. Second, long-term stability in complex aqueous matrices remains inadequate, as issues of metal leaching and active site deactivation have not been fully resolved. Additionally, scalable integration into catalytic devices and economic feasibility in real-world applications represent major bottlenecks. There is still a notable lack of systematic assessment regarding long-term operational performance and cost-effectiveness in continuous-flow reactor systems. Future efforts should prioritize several key directions: (i) Integrating theoretical modeling with experimental validation to guide the rational design of novel MXene supports and multifunctional single-atom sites for precise structural control; (ii) leveraging machine learning to assist in catalyst optimization and high-throughput screening, thereby accelerating the discovery of high-performance materials; (iii) advancing integrated catalytic-separation processes to develop modular and intelligent water treatment systems adaptable to realistic water quality conditions; and (iv) establishing a lifecycle sustainability assessment framework encompassing economic, environmental, and social dimensions to bridge the gap between laboratory research and industrial implementation.

Declaration of competing interest

The authors declare that they have no known competing financial interests or personal relationships that could have appeared to influence the work reported in this paper.

CRediT authorship contribution statement

Zhitong Ma: Writing – review & editing, Writing – original draft. **Yuanfang Wang:** Visualization. **Yajiao Wang:** Writing – review & editing, Writing – original draft. **Xunli Wang:** Data curation. **Qingbai Tian:** Writing – original draft, Visualization. **Xing Xu:** Writing – review & editing, Supervision. **Hanghang Zhao:** Writing – review & editing.

Acknowledgments

The work was supported by National Natural Science Foundation of China (Nos. 42502257, 52500224), the Natural Science Basic Research Program of Shaanxi Province (No. 2025JC-YBQN-434). The authors extend their gratitude to Mr. Qi Chonghua from Scientific Compass (www.shiyanjia.com) for providing invaluable assistance.

Supplementary materials

Supplementary material associated with this article can be found, in the online version, at doi:10.1016/j.cclet.2026.112721.

References

[1] A. VahidMohammadi, J. Rosen, Y. Gogotsi, Science 372 (2021) eabf1581.
[2] L. Jin, S. You, N. Ren, et al., Environ. Sci. Technol. 56 (2022) 11750–11759.
[3] H. Wang, H. Zhang, L. Wang, et al., Chin. Chem. Lett. 36 (2025) 110373.
[4] C. Wu, B. Wang, X. Li, et al., Chin. Chem. Lett. 36 (2025) 111162.
[5] Z. Zhang, C. Zhou, Y. Sun, et al., Appl. Catal. B: Environ. 342 (2024) 123385.
[6] L. Liu, Z. Shen, C. Wang, Chem. Eng. J. 457 (2023) 141327.
[7] P. Yang, Y. Long, W. Huang, et al., Appl. Catal. B: Environ. 324 (2023) 122245.
[8] Y. Zhu, S. Chen, J. Zou, et al., Chin. Chem. Lett. 37 (2026) 112192.
[9] Y. Sun, T. Huang, H. Ji, et al., Chin. Chem. Lett. 37 (2026) 111391.
[10] S. Rao, C. Zhi, X. Wang, et al., J Colloid Interf. Sci. 659 (2024) 594–602.
[11] Y. Wu, G. Huang, K. Zhao, et al., J. Environ. Chem. Eng. 13 (2025) 119388.
[12] C. Jin, D. Sun, Z. Sun, et al., Appl. Catal. B: Environ. 330 (2023) 122613.
[13] Q.V. Ly, L. Cui, M.B. Asif, et al., Water Res. 230 (2023) 119577.
[14] H. Song, L. Chen, Y.H. Xu, et al., Chem. Eng. J. 500 (2024) 156243.
[15] Z. Zhou, F. Yu, J. Ma, Environ. Chem. Lett. 20 (2022) 563–595.
[16] Y. Xin, H. Wang, H. Xue, et al., Appl. Catal. B: Environ. 365 (2025) 124966.
[17] X. Qiao, L. Zhang, Chin. Chem. Lett. 37 (2026) 110998.
[18] W. Wu, W. Zhu, S. Zhao, et al., Appl. Catal. B: Environ. Energy. 366 (2025) 125068.
[19] J. Yang, S. Wang, X. Luo, et al., Chin. Chem. Lett. 36 (2025) 110996.
[20] Y. Gao, Y. Zhou, S.Y. Pang, et al., Water Res. 193 (2021) 116856.
[21] S. Zhang, T. Hedtke, X. Zhou, et al., ACS EST Eng. 1 (2021) 706–724.
[22] C. Yang, C. Zhang, L. Liu, J. Mater. Chem. A 6 (2018) 20992–21002.
[23] R. Song, H. Xie, G. Liu, Chin. Chem. Lett. 36 (2025) 110442.
[24] X. Guo, H. Zhang, Y. Wang, et al., Angew. Chem. Int. Ed. 64 (2025) e202511266.
[25] Y. Zhang, S. Liu, D. Chen, et al., Chin. Chem. Lett. 35 (2024) 108666.
[26] H. Zhao, W. Qi, X. Tan, et al., Chin. Chem. Lett. 36 (2025) 110898.
[27] K. Yin, J. Yang, Y. Li, et al., Chin. Chem. Lett. 35 (2024) 109847.
[28] Q. Tian, B. Yu, Z. Li, et al., Chin. Chem. Lett. 36 (2025) 110322.
[29] X. Lei, H. Zhao, C. Bai, et al., Chin. Chem. Lett. 36 (2025) 111550.
[30] H. Zhao, X. Xu, W. Cui, et al., Adv. Mater. 37 (2025) 2503217.
[31] Q. Tian, X. Xu, X. Duan, Environ. Sci. Technol. 59 (2025) 16823–16826.
[32] Q. Tian, J. Chang, B. Yu, et al., Water Res. 267 (2024) 122488.
[33] Q. Tian, J. Chang, X. Peng, et al., Angew. Chem. Int. Ed. 64 (2025) e202503995.
[34] Q. Tian, Y. Jiang, X. Duan, et al., Water Res. 268 (2025) 122621.
[35] J. Guo, Y. Wang, Y. Shang, et al., Proc. Natl. Acad. Sci. U. S. A. 121 (2024) e2313387121.
[36] H. Lu, L. Hou, Y. Zhang, et al., Water Res. 266 (2024) 122425.
[37] Y. Shang, X. Xu, B. Gao, et al., Chem. Soc. Rev. 50 (2021) 5281–5322.
[38] Y. Shang, Y. Kan, X. Xu, Chin. Chem. Lett. 34 (2023) 108278.
[39] M. Fan, Y. Li, T. Zhang, et al., Water Res. 287 (2025) 124421.
[40] M. Yang, Z. Hou, X. Zhang, et al., Environ. Sci. Technol. 56 (2022) 11635–11645.
[41] L. Hou, S. You, R. Li, et al., Chin. Chem. Lett. 37 (2026) 111903.
[42] S. You, R. Li, H. Lu, et al., Chin. Chem. Lett. 36 (2025) 110955.
[43] C. Meng, S. Zhang, W. Feng, et al., Adv. Funct. Mater. 36 (2026) e15784.
[44] Y. Jiang, D. Baimanov, S. Jin, et al., Proc. Natl. Acad. Sci. U. S. A. 120 (2023) e2210211120.
[45] J. Wang, J. Zhao, S. Wang, et al., Chin. Chem. Lett. 37 (2026) 111859.
[46] H. Wang, X. Li, Y. Deng, et al., Coord. Chem. Rev. 529 (2025) 216462.
[47] M. Sun, S. Chu, Z. Sun, et al., Nano 35 (2024) 382003.
[48] S. Guan, Z. Yuan, Z. Zhuang, et al., Angew. Chem. Int. Ed. 63 (2024) e202316550.
[49] S. Zhou, Y. Zhao, R. Shi, et al., Adv. Mater. 34 (2022) 2204388.
[50] K.C. Chan, X. Guan, T. Zhang, et al., J. Mater. Chem. A 12 (2024) 25165–25175.

[51] H. Gu, W. Yue, J. Hu, et al., Adv. Energy Mater. 13 (2023) 2204014.
[52] M. Kulkarni, A. Lalic, R. Balu, et al., MRS Adv. 9 (2024) 1310–1317.
[53] X. Guo, H. Zhang, Y. Yao, et al., Appl. Catal. B: Environ. Energy 358 (2024) 124432.
[54] Z. Li, X. Ji, Q. Li, et al., Angew. Chem. Int. Ed. 65 (2026) e22714.
[55] L. Chen, Y. Sun, X. Wei, et al., Adv. Mater. 35 (2023) 2300771.
[56] T. Li, L. Yao, Q. Liu, et al., Angew. Chem. Int. Ed. 57 (2018) 6115–6119.
[57] D. Panias, A. Krestou, et al., Powder Technol. 175 (2007) 163–173.
[58] S. Zuo, Y. Ding, L. Wu, et al., Water Res. 231 (2023) 119631.
[59] H. Xu, H. Shou, Z. Yan, et al., Adv. Mater. 37 (2025) 2504586.
[60] D.D. Kruger, H. García, A. Primo, Adv. Sci. 11 (2024) 2307106.
[61] Y. Zou, S.A. Kazemi, G. Shi, et al., EcoMat 5 (2023) e12274.
[62] Y. Jiang, D. Baimanov, S. Jin, et al., Proc. Natl. Acad. Sci. U. S. A. 120 (2023) e2210211120.
[63] S. Zhou, Y. Zhao, R. Shi, et al., Adv. Mater. 34 (2022) e2204388.
[64] W. Peng, J. Han, Y.R. Lu, M. Luo, et al., ACS Nano. 16 (2022) 4116–4125.
[65] M. Ran, H. Xu, Y. Bao, et al., Angew. Chem. Int. Ed. 62 (2023) e202303728.
[66] D. Wang, C. Zhou, A.S. Filatov, et al., Science 379 (2023) 1242–1247.
[67] Y. Bai, G. Zhang, M. Liu, et al., Appl. Catal. B: Environ. Energy 374 (2025) 125378.
[68] D.A. Kuznetsov, Z. Chen, P.M. Abdala, et al., J. Am. Chem. Soc. 143 (2021) 5771–5778.
[69] C. Jin, B. Han, C. Luo, et al., Water Res. 287 (2025) 124420.
[70] C. Zhu, H. Liu, H.Z. Zhang, et al., Water Res. 290 (2026) 125152.
[71] W. Bai, L. Shi, Z. Li, et al., Mater. Today Energy 41 (2024) 101547.
[72] C. Meng, S. Zhang, W. Feng, et al., Adv. Funct. Mater. 36 (2026) e15784.
[73] C. Meng, B. Ding, S. Zhang, et al., Nat. Commun. 13 (2022) 4010.
[74] W. Wang, J. Wei, J. He, et al., J. Colloid Interface Sci. 687 (2025) 677–690.
[75] Z. Yang, Z. Zhou, X. Tan, et al., J. Mater. Sci. Technol. 204 (2025) 224–237.
[76] B. Bhattacharjee, M. Ahmaruzzaman, R. Djellabi, et al., J. Environ. Manage. 324 (2022) 116387.
[77] S. Luo, N. Ma, J. Zhao, et al., Electrochim. Acta 499 (2024) 144712.
[78] Q. Tian, Q. Li, T. Zhang, et al., Adv. Mater. 37 (2025) e09280.
[79] M. Li, P. Wang, K. Zhang, et al., Proc. Natl. Acad. Sci. U. S. A. 120 (2023) e2305705120.
[80] H. Fu, K. Li, Q. Chen, et al., Angew. Chem. Int. Ed. 64 (2025) e202505301.
[81] C. Xu, Y. Huang, R. Xin, et al., Water Res. 283 (2025) 123800.
[82] S. Jiang, W. Xu, Q. Xia, et al., J. Hazard. Mater. 471 (2024) 134309.
[83] H. Chen, R. Wang, Z. He, et al., Chin. Chem. Lett. 37 (2026) 111372.
[84] Y. Ma, J. Wang, S. Huo, et al., Water Res. 287 (2025) 124460.
[85] R. Huang, C. Ma, J. Ma, et al., Water Res. 205 (2021) 117666.
[86] S. Jiang, Y. Zhou, W. Xu, et al., Chem. Eng. J. 486 (2024) 150297.
[87] P. Yin, X. Niu, S.B. Li, et al., Nat. Commun. 15 (2024) 415.
[88] X. Cao, J. Huang, K. Du, et al., Environ. Sci. Technol. 58 (2024) 8372–8379.
[89] M. Li, Q. Wen, Y. Zhang, et al., Water Res. 221 (2022) 118789.
[90] C. Chowdhury, M. Lovato, G. Di Liberto, et al., J. Mater. Chem. A 14 (2026) 5349–5365.
[91] G. Lin, T. Guo, W. Lin, et al., ACS Catal. 15 (2025) 13534–13548.
[92] J. Guo, B. Gao, Q. Li, et al., Adv. Mater. 36 (2024) 2403965.
[93] J. Guo, Z. Gao, T. Zhang, et al., Angew. Chem. Int. Ed. 65 (2026) e23480.
[94] L. Peng, X. Duan, Y. Shang, et al., Appl. Catal. B: Environ. 287 (2021) 119963.
[95] K. Yin, L. Peng, D. Chen, et al., Appl. Catal. B: Environ. 336 (2023) 122951.
[96] K. Yin, R. Wu, Y. Shang, et al., Appl. Catal. B: Environ. 329 (2023) 122558.
[97] Q. Tian, X. Zhang, J. Chang, et al., Water Res. 281 (2025) 123550.
[98] X. Zhao, X. Zhou, Y. Xia, et al., J. Colloid Interf. Sci. 673 (2024) 669–678.
[99] X. Pan, J. Ji, N. Zhang, et al., Chin. Chem. Lett. 31 (2020) 1462–1473.
[100] S. Chen, R. Ding, B. Li, et al., Sep. Purif. Technol. 354 (2025) 129451.